Nanostructured VO₂ (A) and VO₂ (M) Derived from VO₂ (B): Facile Preparations and Analyses of Structural, Thermal, Optical and Thermophysical Properties

Hamdi Muhyuddin BARRA [1] *, **Soo Kien CHEN** [2], **Nizam TAMCHEK** [2],
Zainal Abidin TALIB [2], **Oon Jew LEE** [3], **Kar Ban TAN** [4]

[1] *Department of Physics, Mindanao State University-Main Campus, Marawi City, 9700, Philippines*
[2] *Department of Physics, Faculty of Science, Universiti Putra Malaysia, 43400 UPM Serdang, Selangor, Malaysia*
[3] *School of Fundamental Science, Universiti Malaysia Terengganu, 21300 Kuala Terengganu, Terengganu, Malaysia*
[4] *Department of Chemistry, Faculty of Science, Universiti Putra Malaysia, 43400 UPM Serdang, Selangor, Malaysia*

Vanadium dioxide (VO₂) is an interesting compound that exists in different polymorphic phases with varying characteristics and potential applications. In this study, fabrication and property analyses of three VO₂ polymorphs, namely VO₂ (B), VO₂ (A), and VO₂ (M), are described. Specifically, VO₂ (B) was prepared via hydrothermal method under a low synthesis temperature of 180 °C and a fast processing time of 24 h. In addition, VO₂ (A) and VO₂ (M) were derived from the as-synthesized VO₂ (B) using sequential hydrothermal treatment and calcination process, respectively. From the field-emission scanning electron microscope (FESEM) scans, belt-like VO₂ (B) nanoparticles with dimensions of as low as 35×130 nm^2 were formed. Further, hydrothermal treatment of the as-synthesized VO₂ (B) resulted to a flower-shaped VO₂ (A) due possibly to an oriented attachment mechanism. Meanwhile, annealing of the VO₂ (B) sample caused granular growth that produced plate-like and oblate shaped VO₂ (M) with dimensions of 135 to 306 nm in diameter and 28 to 37 nm in thickness. Moreover, the thermochromic properties of the samples were examined using differential scanning calorimetry (DSC) while the thermophysical properties of the samples were measured via microflash method. Accordingly, the prepared VO₂ (A) and VO₂ (M) samples exhibited phase transition behavior at 168.37 °C and 68.6 °C, respectively. Subsequently, changes in the thermophysical properties of each sample can be observed across the measured transition temperature. In particular, an increase in both the thermal diffusivity and thermal conductivity of VO₂ (M) can be observed when the temperature was raised from 50 °C to 100 °C. On the other hand, there is a noticeable decrease in the thermal conductivity of VO₂ (A) when the temperature was increased from 150 °C to 200 °C.

Keywords: hydrothermal synthesis, nanostructures, thermal conductivity, thermochromic, vanadium dioxide.

1. INTRODUCTION

Vanadium dioxide (VO₂) is a binary compound with unique physical and chemical properties [1]. Hence, it has caught the attention of material scientists and researchers for its functional and industrial applications. Interestingly, VO₂ exists in many polymorphic phases, such as VO₂ (B), VO₂ (A), VO₂ (M), VO₂ (R) and the relatively recent VO₂ (C) and VO₂ (D) [2–4]. Of these polymorphs, VO₂ (M) and VO₂ (R) are considered to be thermodynamically stable and are known to exhibit thermochromic ability [5]. Accordingly, VO₂ (M) undergoes a reversible phase change to VO₂ (R) at a critical temperature of 68 °C [6]. At temperature below τ_c, VO₂ exists in a semiconducting state with a monoclinic crystalline structure; whereas, above τ_c, it becomes metallic with a rutile tetragonal structure [7]. More importantly, this phase transition results to changes in the material's optical, magnetic, electrical and other functional properties [8–10]. For instance, the semiconducting VO₂ (M) is transparent to heat-carrying infrared (IR) radiation while the metallic VO₂ (R) is IR reflectant [11]. Hence, VO₂ (M) is widely considered for potential use in optical switching devices, thermal sensors, electrochromic and thermochromic devices, and as smart window materials

[12–14]. Meanwhile, the metastable phase VO₂ (B) is being examined for its probable application as cathode material due to its layered structure [15]. Previous studies showed that the monoclinic-structured VO₂ (B) has good electrode properties and tunnel functions, which makes it have an excellent Li+ intercalation performance [16–18]. Furthermore, VO₂ (B) can undergo an irreversible phase transition to the thermodynamically stable VO₂ (R) when annealed at high temperature (450 °C or higher) under inert atmosphere or in vacuum [19].

Another VO₂ phase in metastable state is VO₂ (A). Compared with the other VO₂ polymorphs, its phase structure and some physical properties were reported more lately due mainly to the difficulty in its fabrication [20, 21]. It is considered as an intermediate phase between VO₂ (B) and VO₂ (R), and thus, is usually not observed during the synthesis process [22]. However, recent studies revealed that VO₂ (A) can be prepared in nanostructure form using hydrothermal process. In particular, VO₂ (A) can be produced via two-step hydrothermal synthesis using a system temperature of 270 °C [23] or a one-step hydrothermal treatment at a synthesis temperature of 250 °C [21]. In the aforementioned works, divanadium pentoxide (V₂O₅) was used as vanadium source while oxalic acid

---

* Corresponding author. Tel.: +63-955-4204921.
E-mail address: *hmdbarra@msumain.edu.ph* (H.M. Barra)

($H_2C_2O_5$) acted as reducing agent. Another facile way to fabricate VO_2 (A) is by the hydrothermal treatment of VO_2 (B)-H_2O system. This was shown in the work of Zhang and group, wherein VO_2 (B) was dissolved in deionized water and was heated in an electric oven at 280 °C in 48 h [24]. Other studies also investigated the effects of various experimental parameters such as synthesis temperature, pressure as well as process duration on the formation of VO_2 (A) [25]. Interestingly, the few works concerning its property showed that it has thermochromic ability. In the work of Oka and colleague on its thermal properties, it was found that VO_2 (A) undergoes a weak phase transition at a critical temperature of 162.8 °C from a low-temperature phase (LTP-A) to a high-temperature phase (HTP-A) [20]. Further, a follow-through reinvestigation was conducted by Popuri et al. on its crystal structure and phase transition using *in situ* powder X-ray diffraction. Accordingly, it was revealed that the phase transition from LTP-A to HTP-A is first order and reversible, and its structural phase transition temperature is 164.65 °C [21]. Nevertheless, there is a scarcity of research relating to the properties of this polymorph.

In this study, we describe the facile syntheses of nanostructured VO_2 polymorphs. VO_2 (B) nanobelts was produced using hydrothermal method with a low synthesis temperature of 180 °C and a fast duration process of 24 h. Further, VO_2 (A) and VO_2 (M) were derived from the as-synthesized VO_2 (B) via subsequent hydrothermal process and annealing, respectively. In particular, we highlight the preparation of VO_2 (A) via hydrothermal treatment of VO_2 (B)–H_2O system under a low temperature of 180 °C in 24 h. Compared with other works [21 – 24], the present study demonstrates the quickest synthesis of VO_2 (A) under soft conditions. Meanwhile, the VO_2 (M) sample was produced by annealing the as-synthesized VO_2 (B) under N_2 atmosphere. Additionally, analyses of the structural, thermal and optical properties of the VO_2 (B), VO_2 (A), and VO_2 (M) samples were carried out. Furthermore, measurements of the thermal conductivity and thermal diffusivity of the polymorphs were examined. To the best of our knowledge, this is among the first reports on the thermophysical properties of VO_2 (A).

2. EXPERIMENTAL SECTION

2.1. Materials

Divanadium pentoxide (V_2O_5) and oxalic acid ($H_2C_2O_4$) were used as V precursor and reductant, respectively. These chemicals, which were purchased from Sigma-Aldrich, were of analytical grade and used without further purification.

2.2. Synthesis of VO_2 (B)

Preparation of VO_2 (B) sample was done using hydrothermal method. To start the experimental run, the precursor and reducing agent powders were carefully weighed in a semi-micro analytical balance. Specifically, 2.475 g of V_2O_5 in powder form was dissolved in 150 mL deionized water using a magnetic stirrer to make a yellowish solution. Then, 4.950 g of $H_2C_2O_4$ was added while vigorous stirring continued until the mixture turned blue-

green. The change in color implied a reduction of oxidation state from 5+ to 4+. Then, it was transferred into a Teflon-lined steel autoclave with a volume of 240 mL and placed inside an electric oven where it was heated at 180 °C for 24 h. After cooling to room temperature, the precipitate was collected by centrifugation. Then, it was washed with water and ethanol several times to remove any impurities. Finally, the powder was dried overnight at 60 °C. This powder is denoted as as-prepared VO_2 (B) hereinafter.

2.3. Synthesis of VO_2 (A)

To begin the hydrothermal synthesis of VO_2 (A), 1.2 g of the as-prepared VO_2 (B) was dispersed in a beaker containing 120 mL deionized water under magnetic stirring. When the mixture attained good homogeneity, it was transferred into a 240 mL Teflon-lined autoclave. This means that the system had a fill ratio of 0.5. It is then heated at 180 °C for 24 h in an electric oven and cooled naturally. Afterwards, the precipitate was collected, washed with water and ethanol three times, and dried at 60 °C overnight.

2.4. Synthesis of VO_2 (M)

VO_2 (M) was derived from VO_2 (B) via annealing route. First, an amount of the as-prepared VO_2 (B) was heated in a tube furnace under nitrogen atmosphere at a temperature of 650 °C for 2 h. The heating rate was kept at 10 C°/min in the process. The tube was then cooled with the same heating rate to room temperature under nitrogen flow to prevent oxidation.

2.5. Characterization

The phase and crystalline structures of the prepared samples were analyzed using X-ray diffraction (XRD, X'pert Pro PANalytical Philips PW 3040) with a Cu-Kα radiation (λ = 1.54060 Å) generated at acceleration voltage of 40 kV and a current of 40 mA. Also, the data were collected at 2θ scanning range between 20° and 80° with a scanning step rate of 0.017°s⁻¹. Meanwhile, field emission scanning electron microscope (FESEM, JEOL-JSM7600F) was utilized to obtain high-magnification images of the synthesized powders for morphology analysis. Additionally, phase transition behaviors of the samples were investigated using differential scanning calorimetry (DSC, DSC822ᵉ, Mettler Toledo). In particular, the DSC was carried out at a temperature range between 20 °C and 200 °C with a heating rate of 10 C°/min under nitrogen flow. Further, optical properties were examined using a Fourier transform infrared spectrometer (FTIR, Thermo Nicolet 6700) using pelletized KBr. Finally, thermal diffusivity was measured using a light flash apparatus (LFA, Netzsch LFA457) at room temperature (25 °C) to 200 °C. This was done by molding and hydraulic pressing the obtained nanopowder sample into a pellet with a diameter of 10 mm and a thickness of 1 mm.

3. RESULTS AND DISCUSSION

The XRD scans of the prepared samples are shown in Fig. 1 with the corresponding *hkl* values. Firstly, hydrothermal synthesis of VO_2 (B) was effectively carried out as evidenced in the XRD scan of the sample in Fig. 1 a. As displayed in the inset of Fig. 1 a, the peaks of the VO_2

(B) sample's diffractogram matches the VO_2 (B) compound of space group C12/m1 with ICSD code 98-003-1439. In addition, after subsequent hydrothermal treatment of the as-prepared VO_2 (B), the polymorphic phase VO_2 (A) was successfully obtained as indicated in Fig. 1 b. Correspondingly, all peaks can be indexed to VO_2 (A) of space group P42/ncm with ICSD code 98-005-6196 (inset of Fig. 1 b). Meanwhile, the VO_2 (B) powder was converted to VO_2 (M) after the annealing process. This can be inferred from the XRD pattern of the acquired sample as shown in Fig. 1 c. The list of peaks (inset of Fig. 1 c) clearly indicates that no other peaks was observed other than that of VO_2 (M) of space group P121/c1 with ICSD code 98-007-8277. Indeed, it can be seen that all samples exhibited high, sharp and narrow intensity peaks, which denote that the samples are highly pure and well-crystalline.
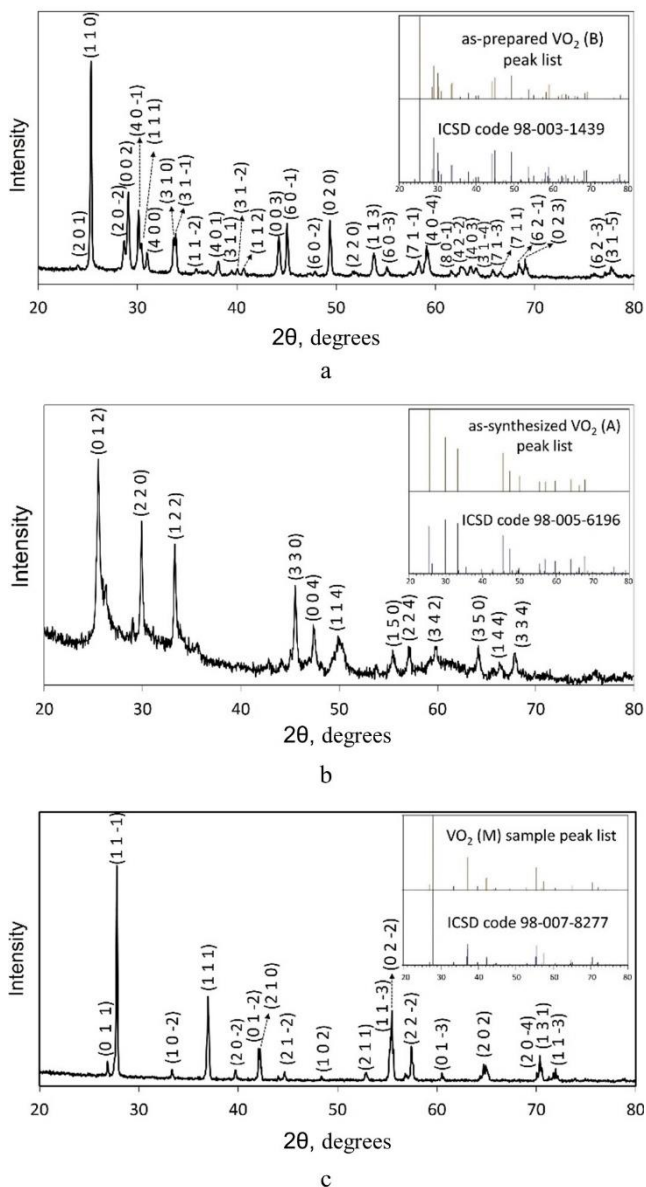

Fig. 1. XRD scans of the prepared: $a - VO_2$ (B); $b - VO_2$ (A); $c - VO_2$ (M) samples. Insets: Peak list of: $a - VO_2$ (B); $b - VO_2$ (A); $c - VO_2$ (M) compounds and the corresponding samples

The FESEM images of the samples are shown in Fig. 2.

After hydrothermal process involving the V_2O_5–$H_2C_2O_4$–H_2O solution, belt-shaped VO_2 (B) was formed (Fig. 2 a). The width and length of the belts were as low as 35 nm and 130 nm, respectively. Additionally, hydrothermal treatment of the as-prepared VO_2 (B) resulted to VO_2 (A) with flower-like shapes (Fig. 2 b). The change in morphology may be due to an oriented attachment mechanism. Firstly, VO_2 (B) nanobelts are broken down during the hydrothermal process.
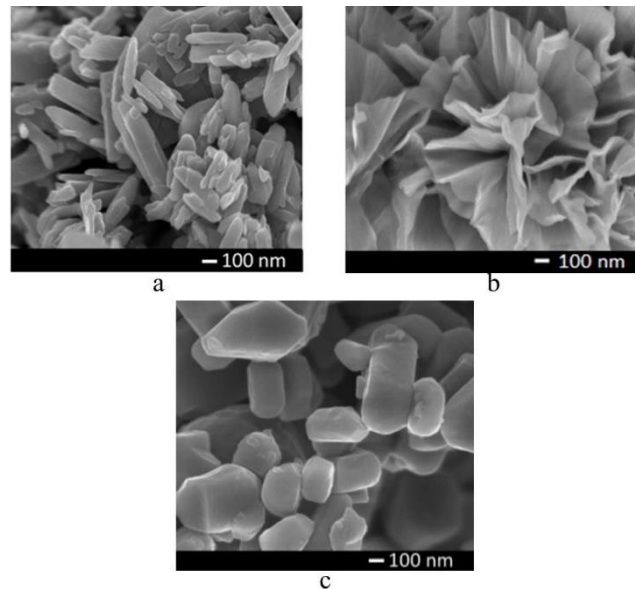

Fig. 2. FESEM images: $a - VO_2$ (B); $b - VO_2$ (A); $c - VO_2$ (M) samples

Subsequently, the nano-sized particles recombine to form nanobelts. Afterwards, these nanobelts would coalesce in a particular direction or orientation to form wider nanobelts or nanosheets due to the prolonged process. Lastly, layer by layer combination of the nanosheets formed the flower-like shape as illustrated in Fig. 2 b. Interestingly, this result is not quite similar with earlier reports. In the work of Xu and colleague, nanorod VO_2 (A) was synthesized via single-step hydrothermal process [22]. Likewise, Zhang fabricated VO_2 (A) nanobelts using two-step hydrothermal method [24]. The differing results may be due to the change in synthetic conditions used in this current study. As elaborated in the works of Ji and colleague, synthetic conditions such as system temperature, duration, and fill ratio or system pressure can affect the growth of VO_2 polymorphs [25]. Meanwhile, after subsequent calcination process, the nanobelt VO_2 (B) sample transformed into plate-like and oblate-shaped VO_2 (M) particles as displayed in Fig. 2 c. This granular growth was mainly due to grain growth mechanism. Correspondingly, there was disordering and breakage of the VO_2 (B) nanobelts due to the dissociation of the V and O atoms. Further, the heat treatment caused reconfiguration of the V-O-based crystals which consequently results in the growth of VO_2 (M) crystalline structure. With the prolonged annealing process, the nano-sized particles coalesce. Finally, agglomeration of the granules led to the formation of grains with oblate and plate-like shapes. Specifically, the dimensions of the synthesized VO_2 (M) powder were 135 to 306 nm in diameter and 28 to 37 nm in thickness.

The phase transition characteristics of the synthesized VO_2 (A) and VO_2 (M) as measured using DSC are shown in Fig. 3. Accordingly, the VO_2 (M) sample displayed a prominent phase transition behavior at 68.60 °C which coincides with the phase transition temperature of bulk VO_2 (M).
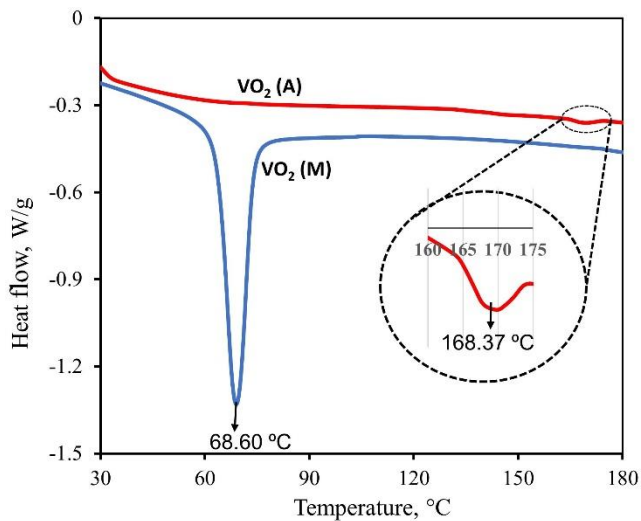

Fig. 3. DSC curves of the VO_2 (A) and VO_2 (M) samples

The enthalpy (ΔH) of the sample was also determined by measuring the area of the curve in the DSC peak to examine the sample's rate of transformation. Correspondingly, the calculated enthalpy of the synthesized VO_2 (M) is 53.77 J/g, which is greater than previous reports [26]. The sample's excellent transition rate may have resulted from its high purity and good crystallinity as seen in its XRD scan in Fig. 1 c as well as its small grain sizes as illustrated in Fig. 2 c. Meanwhile, the VO_2 (A) sample exhibited shift in phase at 168.37°C as displayed by the faint peak in the inset of Fig. 3. Nonetheless, this value is very close to the reported value of the phase transition temperature of VO_2 (A). Also, the measured enthalpy of the sample is $\Delta H=2.55$ J/g, which implies a very weak transformation rate. Indeed, this is consistent with the work of Oka et al., which inferred that the phase transition characteristic of VO_2 (A) is weak [27].

Furthermore, the FTIR spectra of the prepared VO_2 polymorphs are displayed in Fig. 4. The broad absorptions at 3420 cm^{-1} and 1630 cm^{-1} correspond with the stretching and bending vibrations of H_2O, respectively [28]. Also, the peaks at 2918 and 2852 cm^{-1} can be linked with the asymmetrical and symmetrical vibrations of CH_3, respectively, while the 1384 cm^{-1} band indicates the stretching vibration of C-O [29]. It can be noticed that the VO_2 (M) sample has lower peaks in these bands which implies reduction of impurities and H_2O molecules adsorbed on its surface. This is mainly due to the high temperature it was exposed to during the annealing process. In addition, all samples exhibited a double absorption band at 2360 and 2335 cm^{-1} which are associated with the asymmetric vibrations of CO_2 [30]. Meanwhile, the rest of the peaks are characteristic bands of VO_2. Specifically, the absorption band at 1005 cm^{-1} matches the characteristic stretching vibration of short V=O bonds [31]. Below this peak, the differing vibrational modes of the polymorphic phases of VO_2 can be discerned. The 528 cm^{-1} band is attributed to the bending deformation of the V–O–V octahedral in VO_2 (B) [32]. Similarly, the peak at 514 cm^{-1} can be linked to the delocalization of electrons in the V^{4+}–V^{4+} bonds between VO_6 octahedra in VO_2 (A) [29]. On the other hand, the absorption band at 531 cm^{-1} and 674 cm^{-1} are ascribed respectively to the V–O–V octahedral bending mode and the first rutile packing of VO_6 octahedra in VO_2 (M) [28].

Moreover, the thermal diffusivity (α) of the samples as measured using a light flash apparatus is plotted in Fig. 5. Accordingly, from 25 °C to 200 °C, the heat transferring ability of the VO_2 (A) sample slightly decreased from $\alpha_{25°C} = 0.338$ mm^2/s to $\alpha_{200°C} = 0.294$ mm^2/s. Meanwhile, the thermal diffusivity of VO_2 (M) sample has an increasing pattern from room temperature (25 °C) to 200 °C.
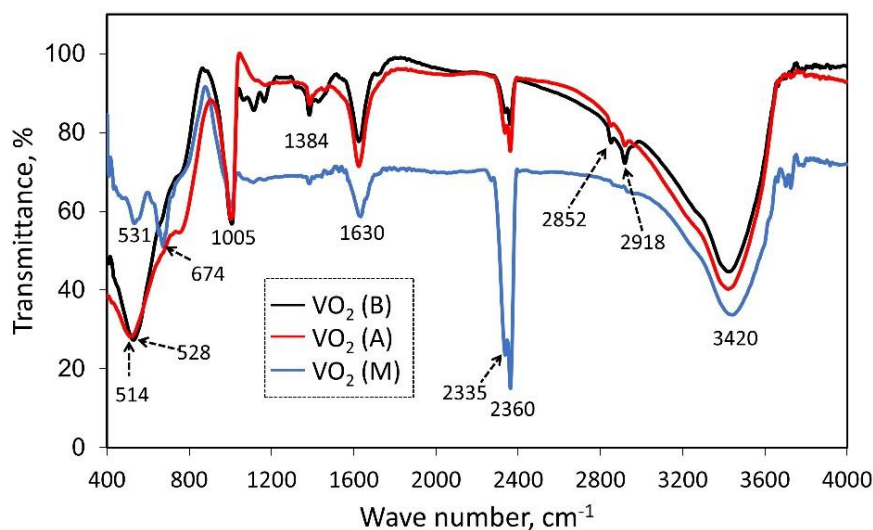

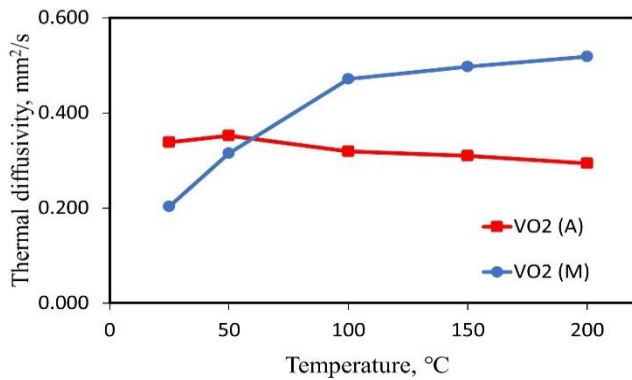**Fig. 4.** FTIR spectra of the synthesized VO_2 (B), VO_2 (A) and VO_2 (M) samples

Fig. 5. Thermal diffusivity of the synthesized VO_2 (A) and VO_2 (M) samples

Moreover, the thermal conductivity (κ) of the samples was calculated using the equation,

$$\kappa = \rho\alpha C_p, \tag{1}$$

where ρ is the material's density, α is the measured thermal diffusivity, and C_p is heat capacity. The measured densities of the pelletized VO_2 (A) and VO_2 (M) samples were 2.98 g/cm^3 and 2.75 g/cm^3, respectively. Inasmuch as these pellets were obtained by hydraulic pressing of nanopowder samples, their densities are lower than the theoretical values. The heat capacities, on the other hand, were determined from the DSC data in Fig. 3. Result of the measurements of κ is plotted in Fig. 6.
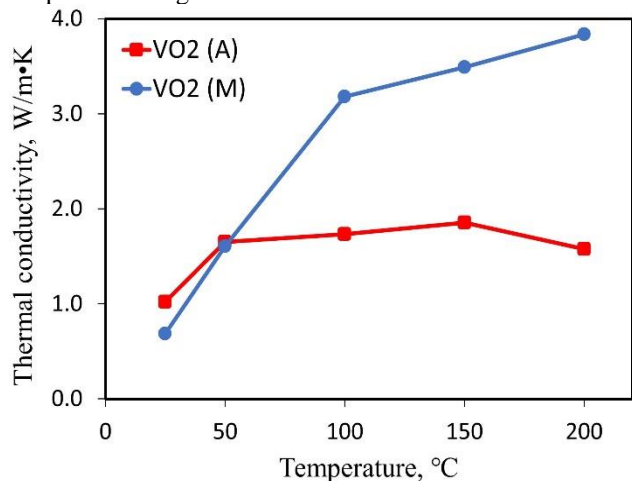

Fig. 6. Thermal conductivity of the synthesized VO_2 (A) and VO_2 (M) samples

It can be seen that the as-synthesized VO_2 (A) exhibits a slight increase in its κ from room temperature ($\kappa_{25°C} = 1.020$ W/m·K) to 150 °C ($\kappa_{150°C} = 1.853$ W/m·K); whereas, after its phase transition, its thermal conductivity decreases to $\kappa_{200°C}=1.577$ W/m·K with $\Delta\kappa =-0.276$ W/m·K. Meanwhile, the profile of the plot of the thermal conductivity of the VO_2 (M) sample is consistent with the results reported by Oh and colleague [33]. Particularly, it is apparent that the thermal conductivity is increasing as the temperature is increased. The changes in thermal conductivity ($\Delta\kappa$) from 25 °C to 50 °C, 50 °C to 100 °C, 100 °C to 150 °C, and 150 °C to 200 °C are 0.92, 1.58, 0.31, and 0.35 W/m·K, respectively. Hence, there is a great increase in κ across the phase transition temperature of VO_2

(M). Interestingly, this value ($\Delta\kappa = 1.58$ W/m·K) is greater than the reported $\Delta\kappa$ for VO_2 bulk and nanobeams [34].

4. CONCLUSIONS

The polymorphic phases of VO_2, namely, VO_2 (B), VO_2 (A), and VO_2 (M) were successfully prepared in nanostructure form. VO_2 (B) was prepared first by a facile hydrothermal synthesis of V_2O_5–$H_2C_2O_4$–H_2O system at 180 °C for 24 h. XRD and FESEM scans of the acquired dark-blue powder exhibited high purity and belt-like shape. Meanwhile, hydrothermal treatment of the as-prepared VO_2 (B) dispersed in H_2O at a low temperature of 180 °C for 24 h with a fill ratio of 0.5 resulted to the formation of VO_2 (A). FESEM image of the sample showed the formation of flower-like shape, while DSC scan displayed a weak phase transition at 168.37 °C. On the other hand, annealing the as-prepared VO_2 (B) at 650 °C for 2 h under nitrogen flow led to its transformation to the thermochromic VO_2 (M) polymorph with plate-like to oblate shape as observed in the FESEM scan. Furthermore, a discernible peak at 68.6 °C from the DSC curve coincides with the known phase transition temperature of VO_2 (M), which is at 68 °C. Meanwhile, the FTIR spectra of the samples showed their differences in the absorption bands particularly in the range between 1000 cm^{-1} and 500 cm^{-1}. Additionally, the thermophysical properties of the VO_2 (A) and VO_2 (M) samples show noticeable changes across their phase transition temperature. Accordingly, a decrease in the thermal conductivity of VO_2 (A) sample can be observed after its phase transition temperature. As for the VO_2 (M) nanopowder, an increase in both its thermal diffusivity and thermal conductivity is evident across its phase transition temperature. For future studies, experiments can be carried out to investigate further the reasoning behind the changes in the thermophysical properties of VO_2 (A) and VO_2 (M) across their corresponding phase transition temperature.

REFERENCES

1. **Ji, S., Zhang, F., Jin, P.** Preparation of High Performance Pure Single Phase VO_2 Nanopowder by Hydrothermally Reducing the V_2O_5 Gel *Solar Energy Materials and Solar Cells* 95 2011: pp. 3520–3526. https://doi.org/10.1016/j.solmat.2011.08.015

2. **Leroux, C., Nihoul, G., Van Tendeloo, G.** From VO_2 (B) to VO_2 (R): Theoretical Structures of VO_2 Polymorphs and *In Situ* Electron Microscopy *Physical Review B* 57 (9) 1998: pp. 5111–5121. https://doi.org/10.1103/PhysRevB.57.5111

3. **Cao, C., Gao, Y., Lou, H.** Pure Single-crystal Rutile Vanadium Dioxide Powders: Synthesis, Mechanism and Phase-Transformation Property *Journal of Physical Chemistry* 112 2008: pp. 18810–18814. https://doi.org/10.1021/jp8073688

4. **Zhang, Y.** VO_2 (B) Conversion to VO_2 (A) and VO_2 (M) and Their Oxidation Resistance and Optical Switching Properties *Material Science-Poland* 34 (1) 2016: pp. 169–176.

https://doi.org/10.1515/msp-2016-0023

5. **Dai, L., Cao, C., Gao, Y., Luo, H.** Synthesis and Phase Transition Behavior of Undoped VO_2 with a Strong Nanosize Effect *Solar Energy Materials and Solar Cells* 95 2011: pp. 712 – 715. https://doi.org/10.1016/j.solmat.2010.10.008

6. **Goodenough, J.** The Two Components of the Crystallographic Transition in VO_2 *Journal of Solid State Chemistry* 3 1971: pp. 490 – 500. https://doi.org/10.1016/0022-4596(71)90091-0

7. **Wegkampf, D., Stahler, J.** Ultrafast Dynamics During the Photoinduced Phase Transition in VO_2 *Progress in Surface Science* 90 2015: pp. 464 – 502. https://doi.org/10.1016/j.progsurf.2015.10.001

8. **Alie, D., Gedvilas, L., Wang, Z., Tenent, R., Engtrakul, C., Yan, Y., Shaheen, S., Dillon, A., Ban, C.** Direct Synthesis of Thermochromic VO_2 Through Hydrothermal Reaction *Journal of Solid State Chemistry* 212 2014: pp. 237 – 241. https://doi.org/10.1016/j.jssc.2013.10.023

9. **Seyfouri, M.M., Binions, R.** Sol-gel Approaches to Thermochromic Vanadium Dioxide Coating for Smart Glazing Application *Solar Energy Materials and Solar Cells* 159 2017: pp. 52 – 65. https://doi.org/10.1016/j.solmat.2016.08.035

10. **Venta, J., Wang, S., Ramirez, J., Schuller, I.** Control of Magnetism Across Metal to Insulator Transitions *Applied Physics Letters* 102 (122404) 2013: pp. 1 – 5. https://doi.org/10.1063/1.4798293

11. **Kiri, P., Hyett, G., Binions, R.** Solid State Thermochromic Materials *Advanced Materials Letters* 1 (2) 2010: pp. 86 – 105. https://doi.org/10.5185/amlett.2010.8147

12. **Yajima, T., Nishimura, T., Toriumi, A.** Positive-bias Gate-controlled Metal-insulator Transition in Ultrathin VO_2 Channels with TiO_2 Gate Dielectrics *Nature Communications* 6 (1) 2015: pp. 1 – 9. https://doi.org/10.1038/ncomms10104

13. **Li, M., Wu, H., Zhong, L., Wang, H., Lou, Y., Li, G.** Active and Dynamic Infrared Switching of VO_2 (M) Nanoparticle Film on ITO Glass *Journal Materials Chemistry* 4 (8) 2016: pp. 1579 – 1583. https://doi.org/10.1039/c5c04046a

14. **Kamalisarvestani, M., Saidur, R., Mekhilef, S., Javadi, F.** Performance, Materials and Coating Technologies of Thermochromic Thin Films on Smart Windows *Renewable and Sustainable Energy Reviews* 26 2013: pp. 353 – 364. https://doi.org/10.1016/j.rser.2013.05.038

15. **Zhang, Y., Huang, Y.** A Facile Hydrothermal Synthesis of Tungsten Doped Monoclinic Vanadium Dioxide with B Phase for Supercapacitor Electrode with Pseudocapacitance *Materials Letters* 182 2016: pp. 285 – 288. https://doi.org/10.1016/j.matlet.2016.07.007

16. **Ni, J., Jiang, W., Yu, K., Gao, Y., Zhu, Z.** Hydrothermal Synthesis of VO_2 (B) Nanostructures and Application in Aqueous Li-ion Battery *Electrochimica Acta* 56 2011: pp. 2122 – 2126. https://doi.org/10.1016/j.electacta.2010.11.093

17. **Zhang, Y., Chen, C., Wu, W., Niu, F., Liu, X., Zhong, Y., Cao, Y., Liu, X., Huang, C.** Facile Hydrothermal Synthesis of Vanadium Oxides Nanobelts by Ethanol Reduction of Peroxovanadium Complexes *Ceramics International* 39 2013: pp. 129 – 141. https://doi.org/10.1016/j.ceramint.2012.06.001

18. **Liu, H., Wang, Y., Wang, K., Hosono, E., Zhou, H.** Design and Synthesis of a Novel Nanothorn VO_2 (B) Hollow Microsphere and Their Application in Lithium-ion Batteries *Journal of Materials Chemistry* 19 2009: pp. 2835 – 2840.

19. **Liu, X., Huang, C., Yi, S., Xie, G., Li, H., Lou, Y.** A New Solvothermal Method of Preparing VO_2 Nanosheets and Petaloid Clusters *Solid State Communications* 144 (5 – 6) 2007: pp. 259 – 263. https://doi.org/10.1039/b821799h

20. **Oka, Y., Yao, T., Yamamoto, N.** Powder X-ray Crystal Structure of VO_2 (A) *Journal of Solid State Chemistry* 86 1990: pp. 116 – 124. https://doi.org/10.1016/0022-4596(90)9121-D

21. **Popuri, S.R., Artemenko, A., Labrugere, C., Miclau, M., Villesuzanne, A., Pollet, M.** VO_2 (A): Reinvestigation of Crystal Structure, Phase Transition and Crystal Growth Mechanisms *Journal of Solid State Chemistry* 213 2014: pp. 79 – 86. https://doi.org/10.1016/j.jssc.2014.01.037

22. **Xu, H., Liu, Y., Wei, N., Jin, S.** From VO_2 (B) to VO_2 (A) Nanorods: Hydrothermal Synthesis, Evolution and Optical Properties in V_2O_5-$H_2C_2O_4$-H_2O System *Optik* 125 2014: pp. 6078 – 6081. https://doi.org/10.1016/j.ijleo.2014.06.132

23. **Ji, S., Zhang, F., Jin, P.** Unexpected Phase Transformation from VO_2 (R) to VO_2 (A) During Hydrothermal Treatment in the V_2O_5-$H_2C_2O_4$-H_2O System *Research on Chemical Intermediates* 37 2011: pp. 493 – 502. https://doi.org/10.1007/s11164-011-0290-2

24. **Zhang, Y., Fan, M., Liu, X., Xie, G, Li, H., Huang, C.** Synthesis of VO_2 (A) Nanobelts by the Transformation of VO_2 (B) under the Hydrothermal Treatment and its Optical Switching Properties *Solid State Communications* 152 (4) 2012: pp. 253 – 256. https://doi.org/10.1016/j.ssc.2011.11.036

25. **Ji, S., Zhang, F., Jin, P.** Selective Formation of VO_2 (A) or VO_2 (R) Polymorph by Controlling the Hydrothermal Pressure *Journal of Solid State Chemistry* 184 2011: pp. 2285 – 2292. https://doi.org/10.1016/j.jssc.2011.06.029

26. **Chen, Y., Zhang, S., Se, F., Ko, C., Lee, S., Liu, K., Chen, B., Ager, J., Jeanloz, R., Eyert, V., Wu, J.** Pressure-Temperature Phase Diagram of Vanadium Dioxide *Nano Letters* 17 (4) 2017: pp. 2512 – 2516. https://doi.org/10.1021/acs.nanolett.7b00233

27. **Oka, Y., Ohtani, T., Yamamoto, N., Takada, T.** Phase Transition and Electrical Properties of VO_2 (A) *Journal of Ceramics Society of Japan* 97 (10) 1989: pp. 1134 – 1137. https://doi.org/10.2109/jcersj.97.1134

28. **Liang, S., Shi, Q., Zhu, H., Peng, B., Huang, W.** One-Step Hydrothermal Synthesis of W-Doped VO_2 (M) Nanorods with a Tunable Phase-Transition Temperature for Infrared Smart Windows *ACS Omega* 1 2016: pp. 1139 – 1148. https://doi.org/10.1021/acsomega.6b00221

29. **Nie, G., Zhang, L., Lei, J., Yang, L., Zhang, Z., Lu, X., Wang, C.** Monocrystalline VO_2 (B) Nanobelts: Large-Scale Synthesis, Intrinsic Peroxidase-like Activity and Application in Biosensing *Journal of Materials Chemistry A* 2 2014: pp. 2910 – 2914. https://doi.org/10.1039/C3TA15051H

30. **Popuri, S.R., Miclau, M., Artemenko, A., Labrugere, C., Villesuzanne, A., Pollet, M.** Rapid Hydrothermal Synthesis of VO_2 (B) and Its Conversion to Thermochromic VO_2 (M1) *Inorganic Chemistry* 52 2013: pp. 4780 – 4785. https://doi.org/10.1021/ic301201k

31. **Botto, I.L., Vassallo, M.B., Baran, E.J., Minelli, G.** IR Spectra of VO$_2$ and V$_2$O$_3$ *Materials Chemistry and Physics* 50 1997: pp. 267 – 270.
https://doi.org/10.1016/S0254-0584(97)01940-8

32. **Valmalette, J.C., Gavarri, J.R.** High Efficiency Thermochromic VO$_2$ (R) Resulting from the Irreversible Transformation of VO$_2$ (B) *Materials Science and Engineering B* 54 1998: pp. 168 – 173.
https://doi.org/10.1016/S0921-5107(98)00148-2

33. **Oh, D., Ko, C., Ramanathan, S., Cahill, D.** Thermal Conductivity and Dynamic Heat Capacity Across the Metal-Insulator Transition in Thin Film VO$_2$ *Applied Physics Letters* 96 (151906) 2010: pp. 1 – 4.
https://doi.org/10.1063/1.3394016

34. **Lee, S., Hippalgaonkar, K., Yang, F., Hong, J., Ko, C., Suh, J., Liu, K., Wang, K., Urban, J.J., Zhang, X., Dames, C., Hartnoll, S.A., Delaire, O., Wu, J.** Anomalously Low Electronic Thermal Conductivity in Metallic Vanadium Dioxide *Science* 355 2017: pp. 371 – 374.
https://doi.org/10.1126/science.aag0410